Impact of data resolution on tracking Southern Ocean cyclones

Article

Accepted Version

Impact of data resolution on tracking Southern Ocean cyclones

Rui Zhong,[a,b] Qinghua Yang,[a,b] Kevin Hodges,[c] Renhao Wu,[a,b] Dake Chen,[a,b]

[a] *School of Atmospheric Sciences, Sun Yat-sen University, Zhuhai, China*

[b] *Southern Marine Science and Engineering Guangdong Laboratory (Zhuhai), Zhuhai, China*

[c] *Department of Meteorology, The University of Reading, Reading, United Kingdom*

Corresponding author: Qinghua Yang, yangqh25@mail.sysu.edu.cn

ABSTRACT

The ERA5 new generation of high-resolution reanalysis provides a possibility to obtain more accurate cyclone tracks in the Southern Ocean. With a commonly used cyclone tracking algorithm, this study evaluates the impact of data resolution on the Southern Ocean cyclone tracks for the period from 1980 to 2020 by pre-processing the ERA5 dataset at different spatial and temporal resolutions. A new track matching method is proposed to assure an accurate comparison of different track data sets, considering the multiple match pairs and best match pair for each track. It is found that the number, distribution, and characteristics of cyclones are considerably different for various resolution scenarios. The higher spatial resolution captures more tracks, while the increased temporal resolution decreases the number, as well as the lifetime and the moving distance of tracks. The shared cyclones of different track data sets show different characteristics, influenced by both spatial and temporal resolutions. Higher spatial resolution schemes tend to identify more additional track points after the overlapping time of shared tracks rather than before. The spatial distribution pattern of additional track points is consistent when increasing temporal or spatial resolution separately. These results are a reference for the application of objective tracking algorithms in the Southern Ocean using input data with higher resolution.

SIGNIFICANCE STATEMENTS

Automatic tracking algorithms are important tools for the research of cyclones and their associated weather phenomena. High-resolution input data are available now for cyclone tracking but it also brings more noise that may affect the results. The problem can be solved by a pre-process (smoothing) process using suitable spatial and temporal resolutions. This study compared the feature of the Southern Ocean cyclones obtained by different spatial and temporal resolution schemes. We further study the shared cyclones in different track data sets with a new track matching method and discuss the different impacts of spatial and temporal resolution, as well as provide a reference for the application and improvement of cyclone tracking in the future.

1. Introduction

Extratropical cyclones are a fundamental weather phenomenon in nature (Schultz et al. 2019), acting as a bridge for the exchange of energy and moisture between the ocean and the atmosphere (Yuan et al. 2009), and between the tropics and the poles (Physick 1981; Boer 1995). The climatology of cyclones is one of the focus topics of cyclone research in the past century (Schultz et al. 2019) and is highly dependent on how cyclones are identified in gridded data and observations. Early studies of cyclone identification were mainly based on synoptic charts or satellite images (Taljaard 1965,1967; Streten and Troup 1973; Carleton 1979) and the results vary among different observers. Thanks to a variety of objective tracking algorithms developed since the 1990s (Alpert et al. 1990; Murray and Simmonds 1991; König et al. 1993; Hodges 1994; Serreze et al. 1995; Blender et al. 1997; Sinclair 1997; Hewson et al. 1997; Schubert et al. 1998; Flaounas 2014), the time-consuming and subjective manual identification of synoptic charts has gradually been eliminated (Murray and Simmonds 1991). Objective cyclone tracking algorithms have been widely used in the identification and tracking of cyclones in the northern and southern hemispheres (Jones and Simmonds 1993; Ueno 1993; Haak and Ulbrich 1996; Hoskins and Hodges 2002, 2005; Wei and Qin 2016; Bauer et al. 2016). They provide a useful tool to obtain the general characteristics of cyclones that have significantly improved our understanding of cyclones and storm tracks.

However, different tracking algorithms introduce uncertainties to the study of cyclone characteristics (Tilinina et al. 2013; Rohrer et al. 2020). Raible et al. (2008) found that the track length and the trend of cyclone characteristics are sensitive to the choice of tracking algorithms, even if they used the same field from the same source. The project Intercomparison of Mid Latitude Storm Diagnostics (IMILAST) was later set up to intercompare the characteristics of cyclones in the northern and southern hemispheres obtained by 15 tracking algorithms (Neu et al. 2013). Their results showed that the characteristics of cyclones are sensitive to different input variables, algorithm settings, pre-processing (noise reduction), and post-processing (track selection) (Rudeva et al. 2014). They suggested that using multi-algorithm ensembles can provide more robustness and reduce uncertainties to some extent (Grieger et al. 2018).

Data from reanalyses, that is often used for cyclone studies, differ in their spatiotemporal resolution, model, and assimilation method and is another source of uncertainty (Hodges et al. 2003, 2011; Bromwich et al. 2007; Allen et al. 2010; Wang et al. 2016; Vessey et al. 2020;

Tilinina et al. 2013). Rohrer et al. (2020) found that cyclone tracking results are strongly dependent on the resolution of input data. The sensitivity of spatial resolution for mesocyclones, medicanes, and polar lows was heretofore highlighted by Zappa et al. (2014). In general, finer temporal resolution brings more fast-moving systems (Pinto et al. 2005) and finer spatial resolution data can identify more weak or small-scale cyclones (Jung et al. 2006). These conclusions promoted a wide use of finer spatial resolutions in cyclone detection and tracking (Simmonds et al. 2008; Tilinina et al. 2014; Di Luca et al. 2015; Wernli and Schwierz 2016). However, the finer resolution also has drawbacks that depend on the input field. Using finer spatial resolution will retain more noise, especially for fields like vorticity. An alternative is to use an inherently smoother field such as the mean sea level pressure (MSLP) field, but some cyclones without a well-defined pressure minimum center or closed isobar cannot be easily found in their early stage, e.g., in the middle latitudes of the southern hemisphere where there are strong pressure gradients. Vorticity or geostrophic vorticity computed from the MSLP (Murray and Simmonds 1991) is a better choice in tracking cyclones within these regions (Sinclair 1994).

Spatial smoothing in the pre-processing before detection and tracking is often applied for fine resolution or noisy fields. For example, spectral filtering is one effective method to reduce sensitivity to spatial resolution and improve tracking reliability (Hoskins and Hodges 2002). Other smoothing methods are also used to avoid bias resulting from different grid spacing such as the constant radius spatial filter used in the work of Sinclair (1997). Indeed, these methods reduce the sensitivity to data resolution in order to better focus the cyclone at particular scales, but different filters can also result in different numbers and locations of tracks (Xia et al. 2012).

Therefore, the sensitivity to different spatial-temporal resolutions and the underlying reasons needs further investigation. Blender and Schubert (2000) provided general thinking about the resolution of input data or pre-processing schemes and introduce a track-matching method that can identify similar tracks in two different track data sets. But the results depend on a choice of parameters for the balance between temporal and spatial matching. The track-matching method developed by Hodges et al. (2011) and Crawford et al. (2021) takes into account the proportion of overlapping points between the paired tracks, providing alternative methods to track-matching. But it should be noted that the proportion of overlapping points may misjudge some track pairings, especially for some long tracks that can match with two or more tracks. Lakkis et al. (2019) designed a method for matching tracks on vertical layers by

linking centers on neighboring pressure levels to find the same cyclone tracked at different layers. The application of track-matching methods will help to identify the different characteristics of paired cyclones and the additional cyclones in track data sets with different spatiotemporal resolutions.

The Southern Ocean is one of the most prominent cyclone activity regions in the world (Jones and Simmonds 1993), providing a large number of tracks for sensitivity research to data resolution. It is also an ideal region with large connected open oceans and less friction and obstruction of terrain compared with the northern hemisphere, which increases tracking stability.

In this study, we examine the sensitivity of cyclone tracking results in the Southern Ocean using the same algorithm but pre-processed (spectral filtering) with different spatiotemporal resolutions based on data from the European Centre for Medium-Range Weather Forecasts (ECMWF) 5th generation reanalysis (ERA5). The ERA5 reanalysis has a higher spatiotemporal resolution than previous reanalyses and allows more details to represent cyclones (Hersbach et al. 2020). Besides, with the help of track matching methods, the tracks obtained by different pre-processing schemes are matched at the same pressure layer. The pairing rates calculated by different matching methods are compared and the characteristics of paired cyclones will be discussed further. The study answers two questions:

(1) What are the differences in the characteristics of the Southern Ocean cyclone tracks obtained by different spatiotemporal resolution pre-processing schemes?

(2) What are the differences in the proportion of shared cyclones and tracks' features among different track data sets?

The paper is organized as follows. Section 2 introduces the reanalysis data used in the objective tracking algorithm and a new track matching method. Section 3 shows the statistical difference between track data sets obtained by different spatiotemporal resolution pre-processing schemes and presents the track matching results between them. In particular, the comparison of the characteristics of shared cyclones could help to understand the impact of different spatiotemporal resolutions. Section 4 summarizes and discusses the main findings of this study.

2. Data and Methodology

a. Data

We use the ERA5 reanalysis (Hersbach et al. 2020) over the period from 1980 to 2020 in this study. The original resolution of ERA5 is TL639L137 (~30 km, 137 vertical levels) with data available at 1 hourly time step. Benefiting from the evolution of the observing system, more observations are actively assimilated by the 4D-Var and land data assimilation systems. The improved IFS Cy41r2 system has helped to reduce biases between the products and observations compared with the older ERA-Interim reanalysis (Berrisford et al. 2011), especially for the temperature, wind, and humidity in the troposphere (Hersbach et al. 2020).

In this study, the data is used at 1-hourly, 3-hourly, and 6-hourly time steps. The main field used for cyclone tracking is the relative vorticity at 850 hPa (ξ_{850}). In addition, the mean sea level pressure (MSLP) at full resolution (0.25° x 0.25°) is used as a reference intensity for the cyclones.

b. Tracking algorithm

The objective cyclone tracking algorithm used is TRACK (Hodges 1994, 1995, 1999). This method can efficiently find the extremum from the mean sea level pressure or relative vorticity fields and track the cyclones in both the northern and southern hemispheres. The tracking process can be divided into three steps, spectral filtering pre-processing, cyclone center positioning, and constructing optimal tracks. More details of the method can be found in Hodges (1994, 1995, 1999).

In this study, the relative vorticity at 850 hPa is chosen as the input field. Strong surface pressure gradients in the mid-latitude region can result in cyclones with no well-defined pressure minimum (open systems) limiting their identification when searching for pressure minima, whereas vorticity-based algorithms can identify cyclones earlier and for more of their lifecycle (Sinclair 1994). However, relative vorticity is a field with a lot of small-scale structures, which can interfere with the tracking of synoptic-scale systems (Gramcianinov et al. 2020). Spectral filtering or smoothing are necessary steps to reduce the small-scale noise for the vorticity field (Hoskins and Hodges 2002).

Three spectral filtering pre-processing schemes are chosen in this study, including T42 (~310 km at the equator), T63 (~210 km at the equator), and T106 (~125 km at the equator), which refer to triangular truncation total wavenumber 42, 63, and 106. Using input reanalysis data with different time steps, we design 9 pre-processing schemes at different spatiotemporal resolution combinations, including 1hT42 / 1hT63 / 1hT106 / 3hT42 / 3hT63 / 3hT106/ 6hT42 / 6hT63 / 6hT106. Parameters that control the local track smoothness and

displacement distances of the tracking algorithm need to be changed to reflect the change in frequency. All schemes output an independent data set of cyclone tracks over the southern hemisphere, including time, latitude, longitude, and intensity (relative vorticity) corresponding to each track point of the cyclone. The tracking is performed on 14-month periods of data from December of the preceding year to January of the following year so that the cross-year track will not be truncated due to insufficient input data. This modification reduces the spurious increase in counts caused by the truncation of cross-year tracks and obtains more accurate counts and lifecycles of cyclones compared with that of 12-month (January to December) data. There is approximately a 6%-10% difference in the number of cyclones in December and January, respectively, between the results of the two different length input data (not shown).

The cyclones born over the Southern Ocean (south of 35°S) are chosen and discussed. Only tracks that last at least 2 days and travel at least 1000 km are involved in the statistical analysis and track matching. The lifespan threshold can eliminate some short-lived systems and noise caused by the algorithms, while the track length threshold can eliminate some systems caused by or trapped by the local orography (Blender and Schubert 2000).

The output vorticity of different spatial resolutions cannot be used as the intensity of cyclones in comparison due to different smoothing levels. Therefore, a full resolution field (MSLP) is used as the reference intensity of cyclones. TRACK is used to search the nearest MSLP minima using B-spline interpolation and steepest descent minimization (Hodges, 1995) for each track center of the tracks and attach it to the tracks. The value at the tracked center is used instead if the nearest MSLP minima cannot be found within a certain range.

c. Statistical method

The spatial statistics for cyclogenesis (the first track point) and activity (all track points) are counted at each Lat-Lon grid (0.25° x 0.25°) in the whole southern hemisphere. The results show the number of track points within a radius of 500 km (Haversine distance) at each grid point. Since each track point may be counted on multiple surrounding grid points, the spatial statistics cannot represent the total number of track points but do show the most frequent areas of cyclone activity. The spatial statistics are normalized for different temporal resolutions.

d. Matching method

Some track matching methods have previously been proposed (Blender and Schubert 2000 [BS2000]; Hodges et al. 2011 [H2011]; Crawford et al. 2021 [C2021]) and revealed good performance in track matching in both hemispheres. The method of BS2000 matches two tracks that are closest to each other, after calculating the Euclidean distance between two track points on the sphere and giving empirical weights for temporal and spatial distance. H2011 and C2021 only match the pairs with a certain percentage or ratio of overlapping points but are different in the calculation for separation distances (4° geodesic distance vs 500 km) and the percentage of overlapping points (50% vs 0.6). It is noted that they don't use a strong restriction "closest to each other" as BS2000. Thus, one track in track data set β is allowed to match with more than one track in track data sets α, leading to an unequal number of pairs between two track data sets when calculating the match rate based on one of them. Actually, having multiple pairs is common when matching two track data sets with large differences in tracked features, such as lifetime and track length. There are no multiple pairs in the results of BS2000 because it only keeps the best/perfect match pairs that are closest to each other. However, the pairs obtained by H2011 and C2021 may not be the best match pairs. The best match pairs do help the feature comparison between paired tracks.

In this study, we want to combine the advantage of previous track matching methods and proposed a new track matching method. It obtains multiple pairings through a recursive procedure and allows a better intercomparison of track data sets obtained from data of different spatial and temporal resolutions in this study. Meanwhile, the strong restriction "closest to each other" as BS2000 can help to choose the best/perfect match pair for each track. The match rates of the new method will be compared with BS2000, H2011, and C2021. The details of the new method are introduced below:

(1) Basic criteria: At least *M* overlapping points meeting a Haversine distance (D_t) of less than 500 km for two tracks.

The number *M* is the daily record frequency, e.g., $M = 4$ for the 6-hourly time step. When matching track data sets with different temporal resolutions, M takes the smaller one of two daily record frequencies. For example, $M = 8$ for the matching between the 3-hour track data sets and 1-hour track data sets. The basic criteria ensure that the two paired cyclones exist simultaneously for at least one day, and their tracks are close to each other during that day.

(2) Mean distance: For each track A in track data set α, $\overline{D_{AB_i}} = mean(D_t,\ t = 1 \ldots\ldots T_i)$, for which B_i is all the track B in track data set β that meet the basic criteria. For each track B in

track data set β, $\overline{D_{BA_i}} = mean(D_t,\ t = 1 \ldots\ldots T_i)$, for which A_i is all the track A in track data set α that meet the basic criteria. T_i is the total number of overlapping points between two tracks. Note that T_i contains all the overlapping points regardless of their distance.

(3) Perfect match (Fig. 1a): For track A and track B, if the minimum $\overline{D_{AB_i}}$ is $\overline{D_{AB}}$ and the minimum $\overline{D_{BA_i}}$ is $\overline{D_{BA}}$, they are defined as a perfect match pair because $\overline{D_{AB}}$ = $\overline{D_{BA}}$. It means track B is the nearest track B_i for track A and track A is the nearest track A_i for track B.

(4) Multiple matches (Fig. 1b): Track B is the nearest track B_i in the track data set β for more than one track in the track data set α. Among them, track A is the perfect match pair with track B (minimum $\overline{D_{AB_i}}$ = minimum $\overline{D_{BA_i}}$), but it caused a mismatch of the other track A_i because minimum $\overline{D_{A_iB_i}} \neq$ minimum $\overline{D_{BA_i}}$. If we mask the perfect match pairs of track B (a recursive procedure) before the matching process of the next track A_i, track A_i can likely be a perfect match pair with track B or other track B', which will increase the pairing rate. This recursive procedure can prevent false negatives (unmatched tracks that should be matched), such as case 1 and case 2 in Fig. 1b, and find the pair for each track that meet the basic criteria as far as possible.

(5) Mismatch: Track A (B) is marked as a mismatched track when there is no track B (A) in the track data set β (α) that meets the basic criteria. Besides, a special case is also marked as a mismatch case because it cannot be identified as a matched track by the recursive procedure (Fig. 1c). No more than four special mismatches occur per data set pairing.

The formula of Blender and Schubert (2000) is used to calculate the match rate.

$$p_a = \frac{N_{perfect} + N_{multi\_\alpha}}{N_\alpha}, p_b = \frac{N_{perfect} + N_{multi\_\beta}}{N_\beta}$$

$N_{perfect}$ is the number of perfect match pairs and the N_{multi_α} (N_{multi_β}) is the number of multiple pairs for track data set α (β), including case 1 and case 2 in Fig. 1b. The p_a (p_b) is given by the ratio of the number of match pairs and the total number N_α (N_β) in track data set α (β). Normally, $p_a \neq p_b$ is due to the different total numbers and the different number of multiple pairs. Note that the individual cases of track data set α (β) are not repeatedly counted even if they have more than one paired case in the other track data set.

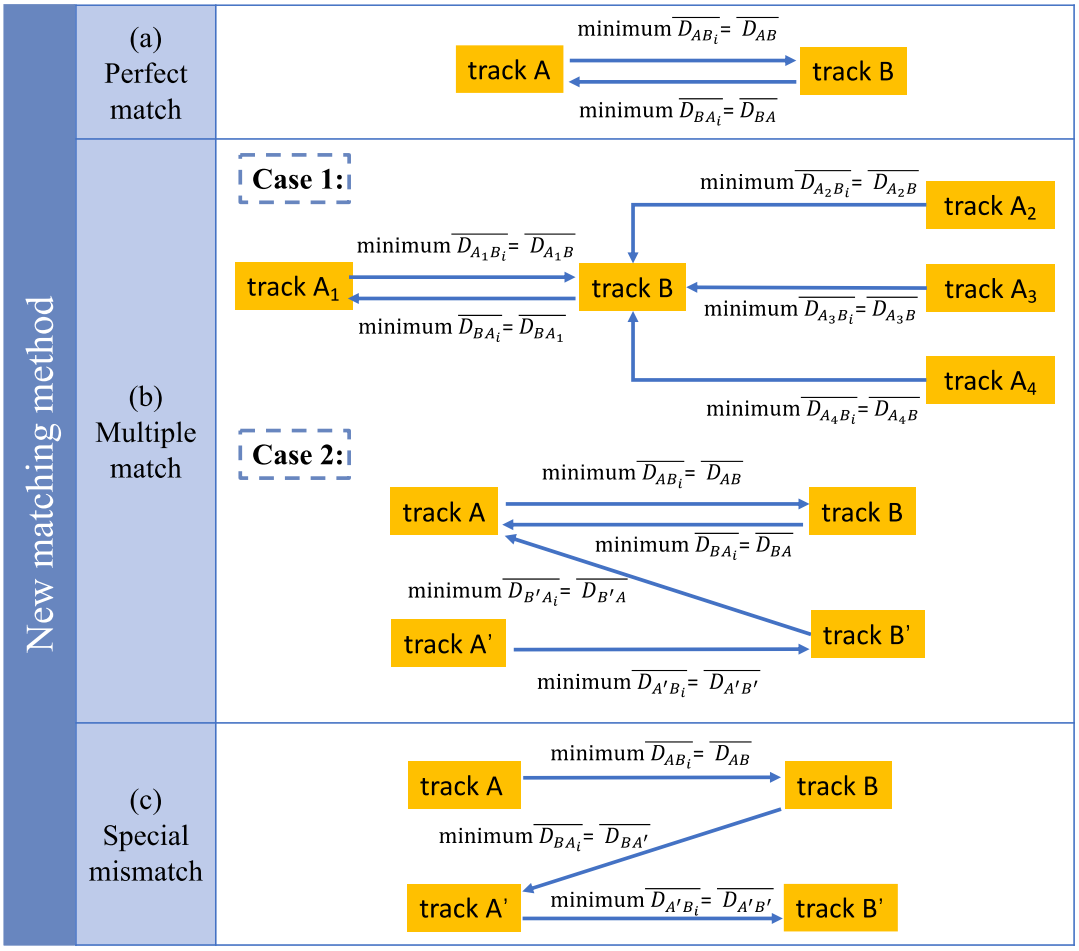

Fig. 1. The schematic diagram of the new matching method. It introduces (a) the perfect match cases, (b) multiple match cases, and (c) a special type of mismatch case. All the track A_i are from track data set α and all the track B_i are from track data set β. The case indicated by the arrow is the nearest track of the case that the arrow starts from. The multiple pairs of tracks in track data set α can only be divided into two types: Case 1 and Case 2.

e. Additional track points

After matching all track data sets to each other, we obtain the match rate and classified the paired and unpaired cases. Especially, the additional points of paired cyclones provide a new perspective to studying the differences caused by resolution. If we take the tracks of 6hT42 as reference tracks, these additional points obtained by higher resolution schemes can be divided into two categories: Front-N (happened before shared time) and Back-N (happened after shared time). Additional track points are only counted compared to their best matching pair, even though some of them may have multiple pairs in other track data sets.

3. Results

a. The effect of spatiotemporal resolution

The Southern Ocean is one of the most active regions in terms of cyclone count in the world. There are about 1000 born over the Southern Ocean at low spatial resolution and over 3000 at high spatial resolution per year (Fig. 2a). The number of cyclones at different spatial resolutions shows a large difference and there are many more cyclones obtained by T106. It is an intuitive result because the finer spatial resolution increases the likelihood of identifying double or multiple centers which can result in broken tracks. Besides, there are more and more mesoscale or small-scale features that can be retained due to the reduced smoothing level at high spatial resolution. The results of high spatial resolution hence show a mixed number of different scale cyclones, not only the synoptic scale cyclones obtained by lower spatial resolutions.

Using finer spatial resolution gets a higher number but using finer temporal resolution gets a lower number, compared with the results of low resolutions. The differences in number at various temporal resolutions increase when using finer spatial resolution, while the differences in number at various spatial resolutions decrease when using higher temporal resolution. This phenomenon also exists in the seasonal variability of cyclone numbers (Fig. 2b) and the meridional distribution of cyclogenesis position (Fig. 2c-d), indicating that the influence of temporal and spatial resolution is interdependent. One probable reason is that the higher frequency increases the probability of identifying transition points between two neighboring tracks, leading to more track splicing which reduces the total number of tracks. The transition points are defined as the connection points between two adjacent tracks (between the cyclolysis point of cyclone A and the cyclogenesis point of cyclone B). They are hard to be distinguished as weakening points of the previous cyclone or strengthening points of the later cyclone or as track points between two strengthening processes of the same cyclone, which highly depend on the frequency and threshold used in the algorithm.

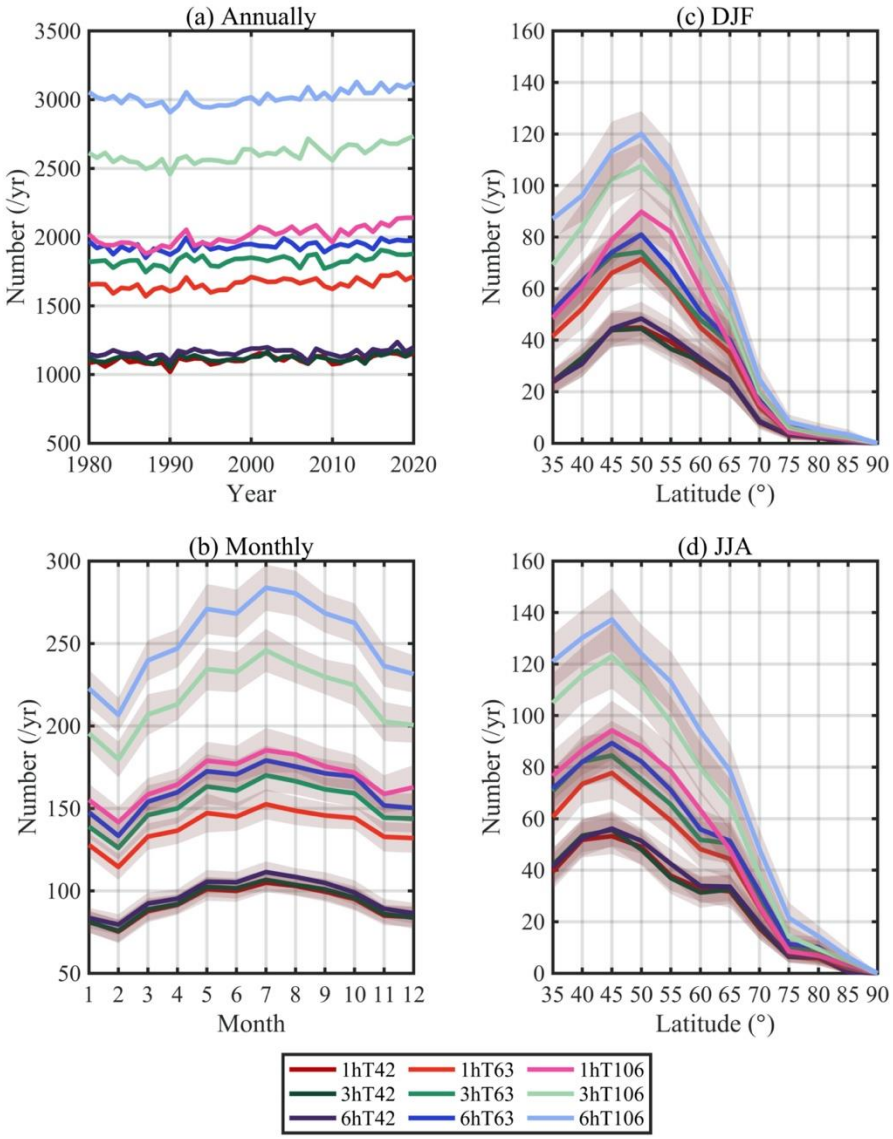

Fig. 2. The (a) annual and (b) the seasonal number of cyclones over the Southern Ocean (south of 35°S). The meridional distributions of cyclogenesis position in (c) DJF and (d) JJA. The results of the same temporal resolution are represented by similar colors (red for 1-hour, green for 3-hour, and blue for 6-hour), and the results of high spatial resolution are represented by light colors. The same is below. The shaded is the standard deviation.

However, this hypothesis cannot fully explain the reduced number of cyclones with increased temporal resolution. Figure 3 shows the difference in features of cyclones obtained by different resolution schemes. The lifetime and moving distance of 3-hour data are always larger than that of 1-hour and 6-hour data (Fig. 3b-c), especially at T42 resolution. The tracks obtained by 3hT42 have the longest lifetime and farthest moving distance, while tracks of 1hT106 get the opposite extreme. There is also a much larger proportion of short-lived and short-distance movement cyclones in the 1hT106 track data set (Fig. 3f & 3g). The shorter

lifetime and moving distance of the cyclones in 1-hour track data sets make them more difficult to pass the chosen track filtering conditions leading to a reduction in the total number, compared with 3-hour track data sets.

The mean lifetime of the tracks of T42 resolution (106.8 hours) is much longer than that of T106 resolution (81.2 hours), indicating that cyclone lifetimes are significantly influenced by spatial resolution. The ranking order of average lifetime of 6-hour and 1-hour track data sets are related to spatial resolutions. Beyond these differences, the mean lifetime of cyclones in different data sets shows consistent seasonal changes which start to get progressively larger in September, reaching a maximum in December and a smaller value from April to September (Fig. 3b). The seasonal variation of moving distance shows an opposite change and the cyclones born in DJF tend to have a longer moving distance. In addition, the difference in moving distance of tracks obtained by different resolution schemes presents interesting results. The tracks in 1hT63 have a similar mean moving distance to that of the tracks in the 6hT63 data set and this also happens between the 1hT106 and 6hT106 data sets.

Although the moving distance and life span show opposite seasonal changes and both of them have great differences across different schemes, the difference in translational speed is small. The cyclones move faster on average during the cold season but the difference is less than 3 $m \cdot s^{-1}$ compared with that born during the warm season. The mean translational speed has less sensitivity to data resolution compared with other features of cyclones. It should be noted that most tracking algorithms apply a search area criterion in the process of linking extreme points, which depends on the frequency of the input data and is also a limitation for maximum translational speed. Therefore, some parameters of the tracking algorithm need to be adapted to the temporal resolution.

The maximum intensity is also an important feature of cyclones. Figure 3a shows the consistent seasonal variation of cyclone intensity among schemes. There is a double peak pattern in seasonal variation in the MSLP of Southern Ocean cyclones, with a relatively high MSLP value in June. The average intensity of cyclones is weak from December to January and reaches the strongest in April and September. This double peak pattern is likely controlled by the semiannual oscillation (SAO) in the southern hemisphere. The SAO has a trough of minimum SLP farthest south and deepest in March and September and farthest north and weakest in June and December (Meehl 1991).

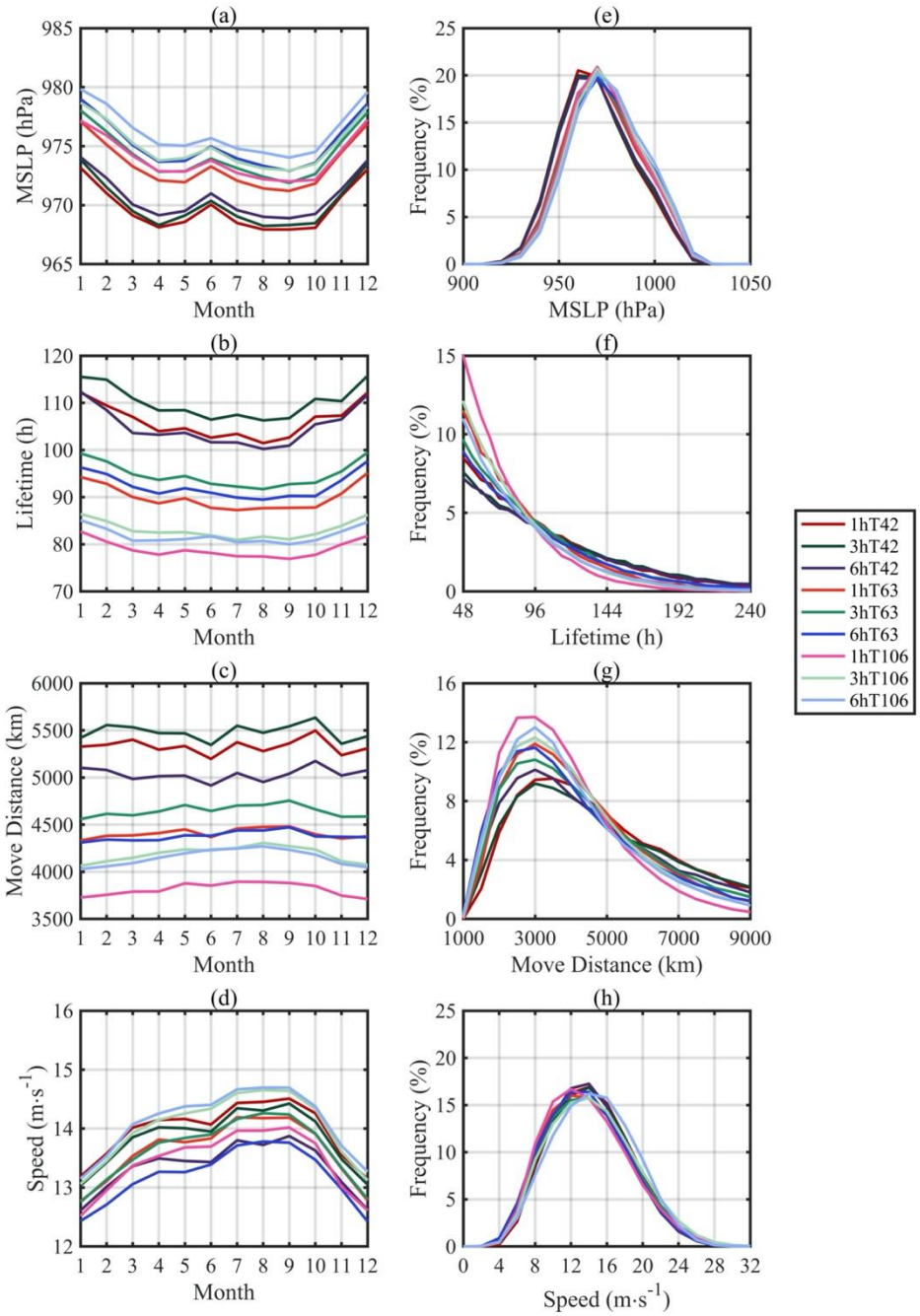

Fig. 3. The mean minimum MSLP, lifetime, moving distance, and translation speed of the cyclones in different track data sets. The first column (a-d) shows the seasonal variation and the second column shows the frequency distribution of different features of cyclones.

The seasonal number of cyclones only shows a consistent single peak pattern (Fig. 2b), with most in winter (JJA, reaching the peak in July) and the least in summer (DJF, reaching a minimum in February). Fig. 2c-d show the meridional distributions of cyclogenesis positions also have significant seasonal variability which is related to the seasonal shift of the polar front and the outer edge of the sea ice. Cyclogenesis occurs mainly between 35°S to 65°S, with a peak latitude moving north in JJA and south in DJF. There is about a 5° difference

between JJA and DJF, which partly comes from the seasonal variation of cyclogenesis over South America and the Southern Atlantic Ocean (Gramcianinov et al. 2019). There are more cyclones born near the east coast of South America in JJA and another center appears at the end of the Antarctic Peninsula (Fig. S1 & S2). There is another weak peak around 65°S except for DJF, which implies active cyclogenesis near the Antarctic coast in the cold season while it is relatively inactive in the warm season. The number of cyclogenesis events near the Adélie Land during DJF is much less than that in JJA (Fig. S1 & S2), especially in the results of low spatial resolution. The seasonal variations in the intensity and the stability of the wind direction of katabatic winds may affect the cyclogenesis in this region where the relationship between katabatic winds and mesoscale cyclogenesis has been explored extensively (Carrasco et al. 2003). Besides, it is noted that the results of different temporal resolutions are more similar in DJF, while they are differing more in JJA, indicating that there may be seasonal differences in the impact of temporal resolution. The between-scheme differences have a weak seasonal variation, especially for the results of the three different temporal resolutions under the same spatial resolution (Fig. S1 & S2).

In general, the distribution of high-frequency areas of annual cyclogenesis is consistent across different schemes (Fig. 4). One is located in the eastern coastal region of South America (50-70°W, 40-55°S), which is also found by the MSLP-based tracking algorithms (Wernli and Schwierz 2006) and geostrophic vorticity-based tracking algorithms (Jones and Simmonds 1993; Simmonds et al. 2003). The leeward side of the Andes in South America is prone to cyclones associated with the subtropical jet. Some cyclones decay on the upslope and regenerate on the downslope side of the Andes (Hoskins and Hodges 2005). More than that, several sub-regions of the coast of South America and the Southern Atlantic Ocean have different cyclogenesis mechanisms (Gramcianinov et al. 2019). The circumpolar trough is the main area of cyclogenesis, with a large number of eastward-moving cyclones (Jones and Simmonds 1993). The area northeast of the tip of the Antarctic Peninsula, to the east of the Drake Passage, is another high-frequency region (Turner et al. 1997), which is also confirmed by Sinclair (1995). Turner et al. (1997) also concluded six types of cyclogenesis in this region, such as developments within a trough, on a (pre-existing) front, leeward forming, and in isolation. Some of these events consist of mesoscale disturbances which have a poor representation in coarse spatial resolution.

The other high-frequency area is located off the Adélie Land coast (140~160°E, 60~70°S). The mesoscale cyclone activity is considered to be one of the reasons for the

frequent cyclogenesis in this region (Claud et al. 2009). The unique juxtaposition of the extraordinary katabatic wind regime and dissipating synoptic-scale cyclones to the west make cyclogenesis frequent near the Adélie Land (Bromwich et al. 2011). The active synoptic-scale cyclones in this region make it the second-highest value in the results of T42 resolution. In addition, the high-frequency cyclogenesis area near New Zealand (170-180°E, 40-50°S) and the east coast of Australia (120°E, 40-50°S) become more obvious with the increase in spatial resolution. Some sub-tropical cyclones (e.g., east coast lows) which are considered to be a kind of mesoscale cyclone are active in the latter regions (Dowdy et al. 2019). The same change happens in the last high-frequency region located in the Southern India Ocean (60-110°E, 45-55°S) which is considered the core region of the subpolar jet streams. Eddy activity in the upper and lower troposphere over the eastern South Atlantic and the Indian Ocean is strong throughout the year (Nakamura and Shimpo 2004). Besides, the strongest meridional sea surface temperature (SST) gradient associated with an oceanic frontal zone over the southwestern Indian Ocean is a favorable condition for cyclogenesis (Sinclair 1995). Note that this cyclogenesis region is not prominent in the results of 1hT42 compared with other high-frequency regions but it becomes more noticeable when increasing the spatial resolution and decreasing the temporal resolution.

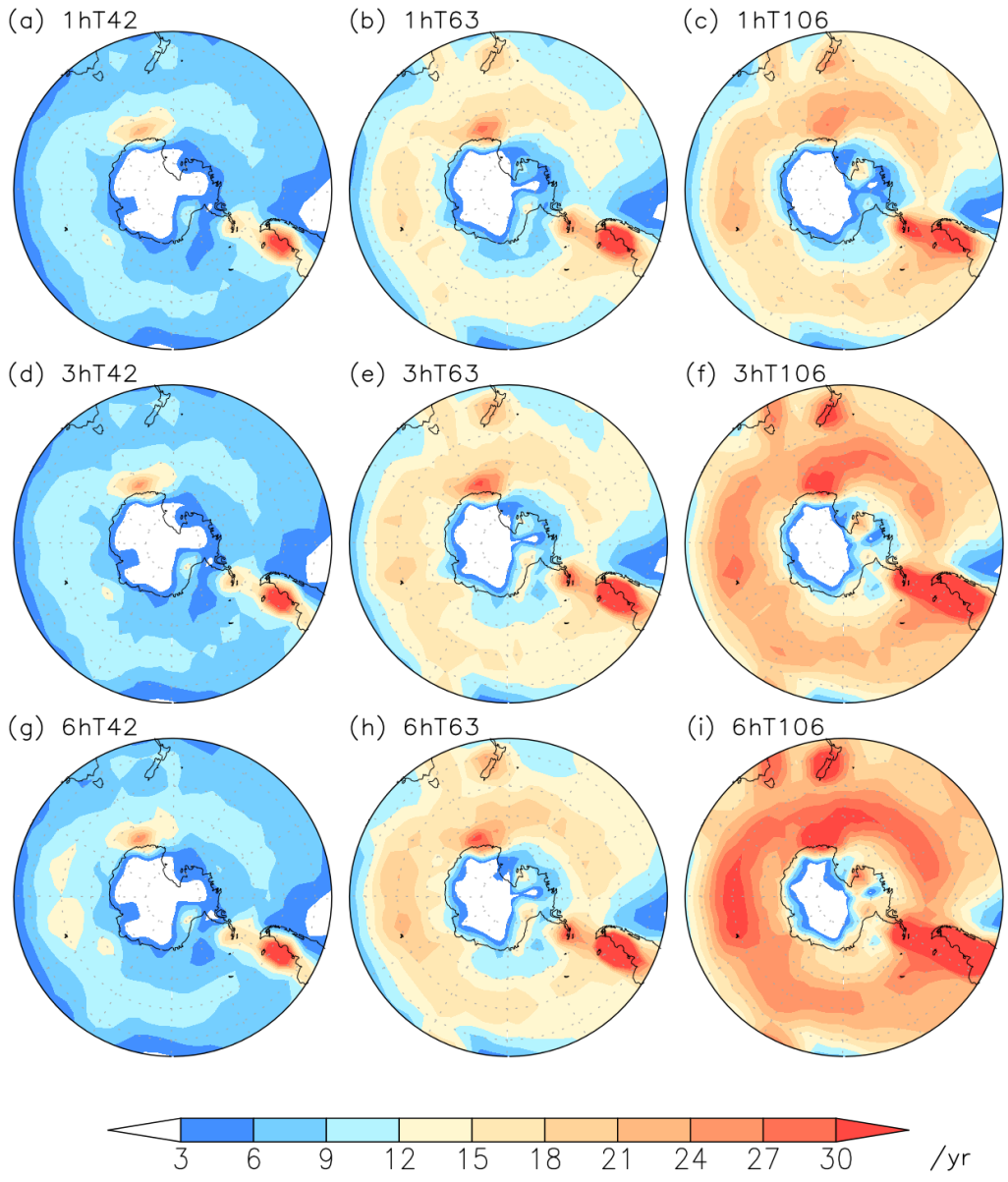

Fig. 4. The spatial pattern of cyclogenesis over the Southern Ocean (south of 35°S). The shaded shows the number of cyclogenesis events (first track point) counted in a 500 km radius around grid points per year.

Figure 5 shows the feature density of cyclone track points over the Southern Ocean, containing the track points belonging to the cyclone formed south of 35°S. The results show that there is an annular but unevenly high-value area around Antarctica with more frequent cyclonic activity in the region (90°E -120°W, 60-65°S) on the west side of the Antarctic Peninsula to the Drake Passage. The former is also one of the main cyclogenesis regions mentioned above, and most of the cyclones in the circumpolar trough have an eastward movement after formation. The background westerly wind begins to slow down in these areas, as well as the average speed of the cyclone (not shown). The latter is due to the

obstruction of terrain, which slows down the speed of cyclones moving to this place in the Bellingshausen Sea (Chen et al. 1989). The pattern above is similar across the results of the different schemes. Larger values can be seen in the results of finer spatial resolution because of the number of additional tracks (Fig. 2a), but the results of 1-hour data only have a slight change when the spatial resolution increases (Fig. 5a-c).

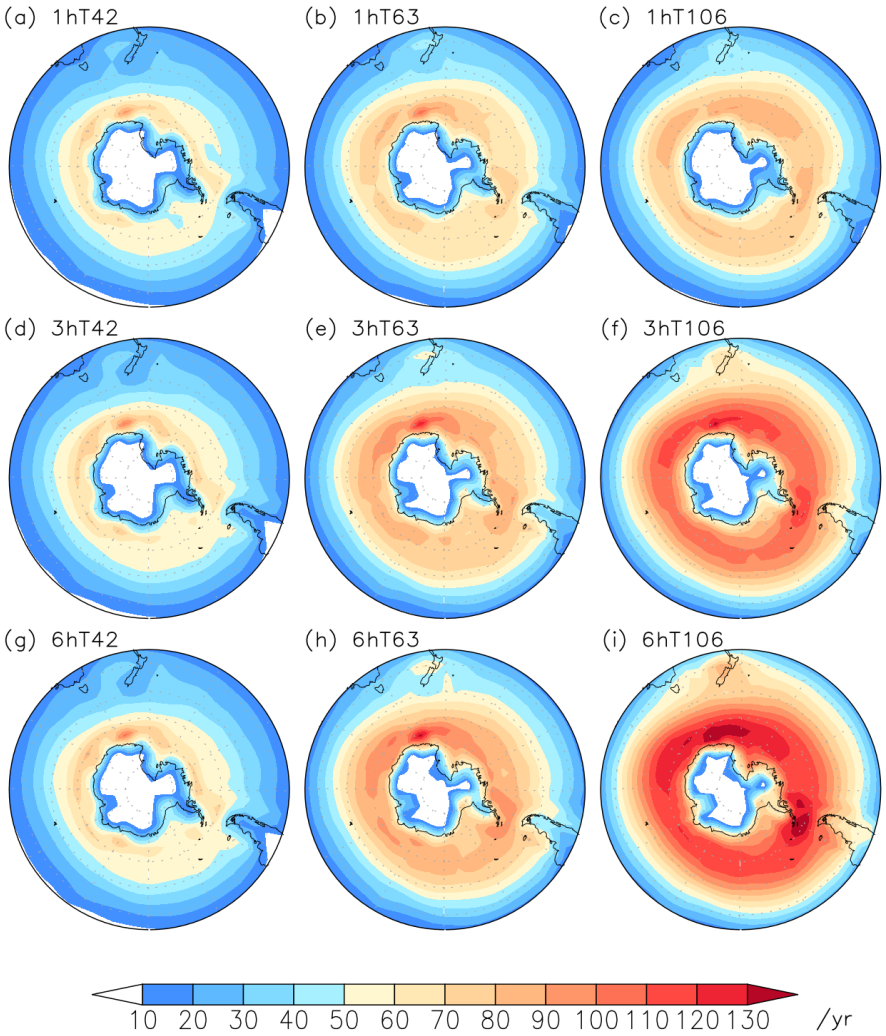

Fig. 5. The spatial feature pattern of cyclone track points over the Southern Ocean (only contains the track points of cyclones that formed south of 35°S). The shaded shows the number of track points counted in a 500 km radius around grid points per year.

b. Track matching results

To further examine the effect of spatial and temporal resolution on the tracking, a track matching method is used to pair the same or most similar tracks in each track data set. The

multiple pairings between the tracks data sets obtained by different resolution schemes will be considered in this section.

Table 1. The multiple pairing results between track data sets of different spatiotemporal resolutions and the reference 6hT42 track data set. The results of the pairing after exchanging track data set α and β are shown in the last two columns. The number in the brackets is the proportion of multiple pairs.

Pairs	α (1) & β (1)	α (1) & β (≥2)	β (1) & α (1)	β (1) & α (≥2)
α (1hT42) & β (6hT42)	39710	958 (2%)	38552	2112 (5%)
α (1hT63) & β (6hT42)	38049	1232 (3%)	31187	8170 (21%)
α (1hT106) & β (6hT42)	36464	728 (2%)	25386	11854 (32%)
α (3hT42) & β (6hT42)	40742	1629 (4%)	41258	1109 (3%)
α (3hT63) & β (6hT42)	38896	1806 (4%)	32443	8417 (21%)
α (3hT106) & β (6hT42)	39653	1080 (3%)	25581	15313 (37%)
α (6hT63) & β (6hT42)	39448	1770 (4%)	32662	8714 (21%)
α (6hT106) & β (6hT42)	39949	1284 (3%)	24777	16712 (40%)

Table 1 shows the multiple pairing results between different cyclone track data sets for the different spatiotemporal resolution schemes and the reference 6hT42 track data set, and groups them according to the number of paired cyclones. Most of the pairs are single pairs and part of the pairs are multiple-pairings, which are obtained by the recursive procedure of the new track matching method. The proportion of multiple-pairings is usually under 5% except for the matching results between two track data sets with different spatial resolutions. Besides, it can be found that the proportion of multiple pairs depends on the choice of the track data set α and β. Although they get a similar number of paired cyclones, they get a different proportion of multiple pairs if two track data sets are swapped as a baseline data set. The tracks in the baseline data set are only paired once. In general, the proportion of multiple pairs depends on the feature differences of cyclones between two track data sets, such as lifetime and moving distance (Fig. 3). A cyclone with a long lifetime is more likely to have multiple pairs (example in Fig. 6).

To better visualize the effect of spatial and temporal resolution on the tracks of the cyclone, Figure 6 shows an example of the paired cyclone in different track data sets. The 3hT42 scheme gets the longest track (B2) which starts at 102.7°E and ends at 92.7°W, with the longest lifetime (183 hours). It is matched with the second-longest track (A1) from the 1hT42 data set, but A1 undergoes cyclolysis earlier at 109°W. The same track is divided into

two tracks in the 6hT42 data set (C2 and C8). The start point of C2 is east of that of tracks in other data sets, indicating that the decrease in temporal resolution will delay the identification of the cyclogenesis points. The same phenomenon can also be seen in the pairs (A4, B4, C4) and the pairs (A9, B10, C10) at T106 resolution. There is greater uncertainty in the influence of spatial resolution. Some tracks in finer spatial resolution have an earlier cyclogenesis point, such as B5 and B6, C1 and C3, C5 and C7, while there are opposite situations, such as A2 and A3, B9 and B10, indicating uncertainty in the effect of spatial resolution on the identification of cyclogenesis points. In addition, several tracks in high resolutions that only have a part of tracks close to the track of the T42 data set are also paired by the new method. Based on the overlapping segments between them occurring at different times in the cyclone's lifespan, these kinds of tracks can be divided into two groups: split pairs and merge pairs. The split pairs (e.g., C5 and C6) generated within a neighborhood gradually move away from each other in the second half. They generally come from the same polycentric cyclones or the same front of cyclones. The merge pairs (e.g., B7 and B9) generated in two locations that are far apart are close in the second half. Similar phenomena are more likely to occur as the spatial resolution increases.

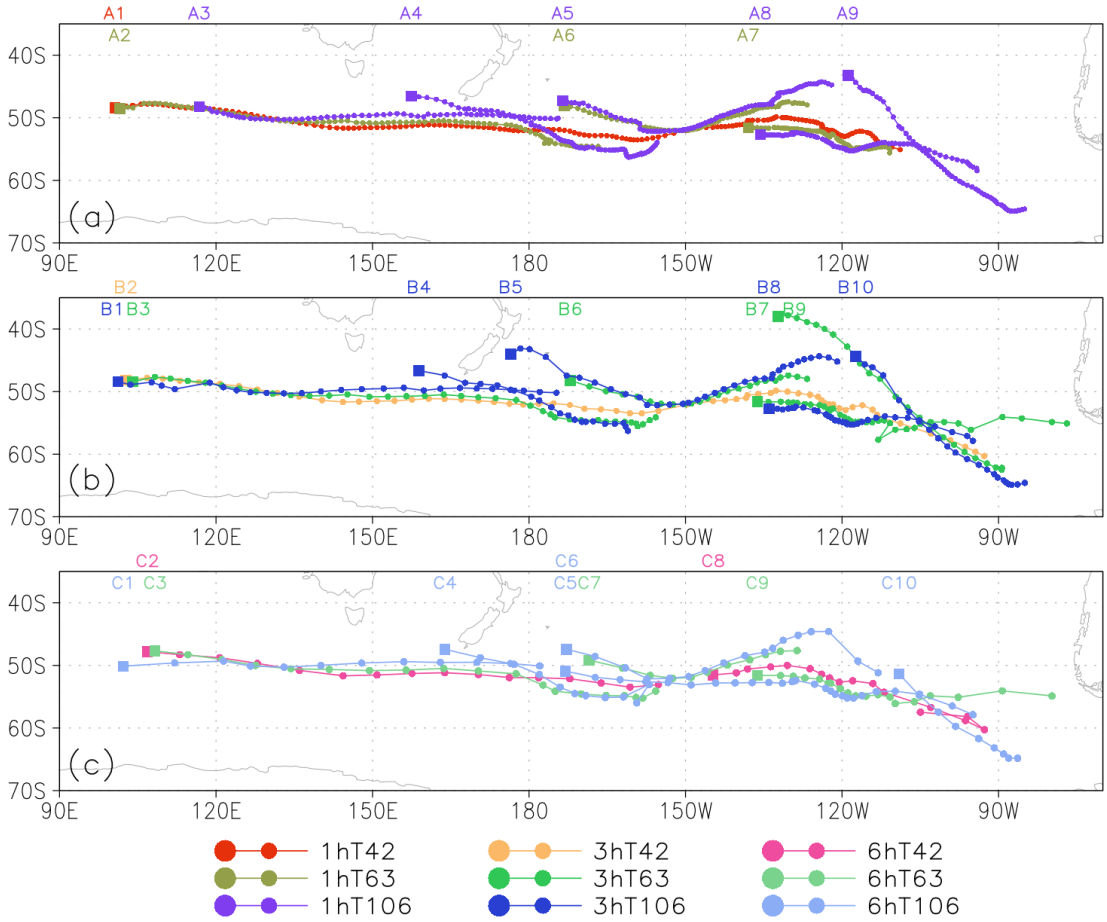

Fig. 6. An example of the paired cyclone in different track data sets is found by the new track matching method. They are shown in three groups and the track in each group comes from the track data sets with the same temporal resolution. (a) 1-hour, (b) 3-hour, (c) 6-hour. The longest track comes from the 3hT42 track data set, which is the best match pair for all other tracks.

After additionally considering the multiple pairs, the pairing rate between each track data set is shown in Figure 7. Compared with the results of BS2000, the pairing rate of the new method is higher for each matching group. Apart from the fact that the new method takes into account multiple pairings, another reason for this is that BS2000 uses the spatiotemporal weighted Euclidean distance of the whole track for pairing. The results of BS2000 depend on the choice of weights which are chosen rather subjectively. In addition, the Euclidean distance is not ideal for spherical data due to the converging meridians in high latitude regions. When applying this method in practice, it was not ideal for pairing cyclones with large differences in their lifetime. The lifetime affects the pairing of some cases, resulting in mismatches.

(a) New method										
Unit /%	**1hT42**	**3hT42**	**6hT42**	**1hT63**	**3hT63**	**6hT63**	**1hT106**	**3hT106**	**6hT106**	**Number**
1hT42		97	94	86	90	91	80	88	90	45434
3hT42	92		95	86	90	91	80	88	90	45842
6hT42	88	93		85	89	91	80	88	89	47564
1hT63	68	71	72		96	92	75	85	86	68028
3hT63	63	67	68	83		92	72	83	85	75035
6hT63	61	64	65	76	87		69	81	84	79329
1hT106	60	63	65	68	75	77		93	88	82482
3hT106	54	57	59	61	69	72	70		86	106705
6hT106	50	53	53	54	62	65	57	74		123731
(b) BS2000										
Unit /%	**1hT42**	**3hT42**	**6hT42**	**1hT63**	**3hT63**	**6hT63**	**1hT106**	**3hT106**	**6hT106**	**Number**
1hT42		79	71	61	63	63	63	68	71	45434
3hT42	78		77	60	62	63	62	67	70	45842
6hT42	68	74		59	61	62	62	67	69	47564
1hT63	41	40	41		73	65	56	62	64	68028
3hT63	38	38	39	67		69	53	59	61	75035
6hT63	36	36	37	56	65		51	58	60	79329
1hT106	35	35	36	46	48	49		70	63	82482
3hT106	29	29	30	40	41	43	54		59	106705
6hT106	26	26	27	35	37	38	42	51		123731

Fig. 7. The pairing rate (percentage on shading) between different track data sets using the track matching method of (a) new track matching method and (b) BS2000. The upper right corner of the diagonal is p_a and the lower right corner is p_b. Each pairing rate uses the track data set of the row label (baseline track data set) as the denominator of the formula calculating the pairing rate.

The pairing rate of the new method is also compared with the results of H2011 and C2021, using the same proportion of overlapping points in their works (≥50 % for H2011 and ≥0.6 for C2021). Their results between two track data sets with the same spatial resolution are close to that of the new method but their results between two track data sets with different spatial resolutions are smaller than that of the new method. Considering these proportions may not be optimal in different regions, Figure 8 shows the pairing rate of H2011 and C2021 when reducing the proportion to 0 (>0) are shown in Figure 8b and 8d. It can be found that the pairing rates of H2011 and C2021 increase when loosening the limitation of proportion. It is noted that both H2011 and C2021 include all pairs that meet the criteria. There are multiple pairings for some cyclones, but they are only calculated once into the pairing rate. Otherwise, the pairing rate may exceed 100%. The difference is that the track matching scheme of C2021 based on H2011 has a looser mean separation distance threshold (500 km) and a stricter limitation on the minimum proportion of overlapping points. For both of them, a suitable mean separation distance and limitation on the minimum proportion of corresponding points need to be selected based on the characteristics of the pairing track data sets.

(a) H2011, ≥ 50%										
Unit /%	1hT42	3hT42	6hT42	1hT63	3hT63	6hT63	1hT106	3hT106	6hT106	Number
1hT42	0	96	94	77	84	84	63	74	73	45434
3hT42	92	0	95	80	84	84	69	76	75	45842
6hT42	87	92	0	80	84	84	69	76	75	47564
1hT63	55	63	65	0	95	92	70	82	81	68028
3hT63	54	59	60	83	0	92	69	80	80	75035
6hT63	52	56	57	75	86	0	66	77	78	79329
1hT106	37	47	49	60	71	72	0	92	86	82482
3hT106	36	41	43	55	64	66	69	0	85	106705
6hT106	31	35	36	47	55	57	55	72	0	123731
(b) H2011, > 0%										
Unit /%	1hT42	3hT42	6hT42	1hT63	3hT63	6hT63	1hT106	3hT106	6hT106	Number
1hT42		96	94	84	86	86	73	78	77	45434
3hT42	92		95	82	85	85	72	77	75	45842
6hT42	87	92		81	84	85	71	77	75	47564
1hT63	64	66	66		95	92	75	83	82	68028
3hT63	58	60	61	83		92	71	81	80	75035
6hT63	55	57	58	75	86		68	78	78	79329
1hT106	50	50	51	68	72	74		93	87	82482
3hT106	42	43	43	59	65	66	70		85	106705
6hT106	35	36	37	50	56	57	57	73		123731
(c) C2021, ≥ 0.6										
Unit /%	1hT42	3hT42	6hT42	1hT63	3hT63	6hT63	1hT106	3hT106	6hT106	Number
1hT42		96	94	74	87	88	60	82	83	45434
3hT42	92		95	82	89	89	75	86	87	45842
6hT42	87	92		82	88	89	76	86	87	47564
1hT63	51	67	69		95	92	66	83	84	68028
3hT63	56	64	65	83		92	70	83	84	75035
6hT63	54	61	63	75	87		68	81	84	79329
1hT106	35	55	58	56	73	75		93	87	82482
3hT106	41	52	54	56	68	71	70		87	106705
6hT106	37	45	48	50	60	64	56	74		123731
(d) C2021, > 0										
Unit /%	1hT42	3hT42	6hT42	1hT63	3hT63	6hT63	1hT106	3hT106	6hT106	Number
1hT42		97	94	87	90	90	81	88	89	45434
3hT42	92		95	86	89	90	80	87	88	45842
6hT42	88	93		85	89	90	80	87	88	47564
1hT63	69	70	71		96	92	77	86	87	68028
3hT63	63	65	66	83		92	73	84	85	75035
6hT63	60	62	63	76	87		70	82	84	79329
1hT106	60	61	62	71	76	78		93	89	82482
3hT106	53	54	55	63	69	72	71		87	106705
6hT106	46	48	49	56	62	64	59	75		123731

Fig. 8. The pairing rate (percentage on shading) between different track data sets using the track matching method of (a-b) H2011 and (c-d) C2021. The results of the commonly used proportion of overlapping points are shown in (a) for H2011 (≥ 50%) and (c) for C2021 (> 0.6). Similar results after reducing the limitation of proportion to 0 (> 0) are shown in (b) for H2011 and (d) for C2021.

Although the basic criteria of the new method also contain two thresholds (500 km and one day), it has more universal applications. The distance of 500 km is a suitable distance threshold for the track matching between two track data sets obtained by different spatial resolution pre-processing schemes or different objective tracking methods. It is also a typical radius distance of a cyclone. The time thresholds of one day ensure that the two paired

cyclones exist simultaneously for at least one day, and each of their overlap points is close to each other during that day. One day is a suitable shared time for cyclones with a lifetime of at least two days which is a typical filtering setting for synoptic systems used in most automatic algorithms. These two thresholds can be changed according to the size and lifetime of different sizes of cyclones. It can also reduce the workload of investigating the optimal limitation on the proportion of overlapping points. The recursive procedure can obtain the multiple pairings ignored by some track matching methods, which can reduce the mismatch rate for two track data sets with large uncertainty. This uncertainty may arise from spatiotemporal resolution, algorithm settings, different fields, etc. In addition, using the mutual-closest condition for pairing can get the best match pairs, which is beneficial for the comparison of the characteristics of the paired cyclones.

c. Features of shared cyclones

The shared cyclones in each track data set are obtained by the new track matching method. In general, they have different features in different track data sets due to the additional track points resulting from different resolutions. The track points before the overlapping points are recorded as Front-N, and the track points after the overlapping points are recorded as Back-N. Figure 9 shows the relative difference in the proportion of the additional track points based on the results of Figure 5. It can be found that the additional track points of shared cyclones show a largely different pattern before and after the overlapping stage. There are more Front-N located in the mid-latitudes of the Southern Indian Ocean and the leeward of Andes, while the Back-N is mainly distributed in the coastal Antarctic continent, except the Weddell Sea. The number of Back-N is more than that of Front-N in Figure 9, indicating that the increase in temporal resolution mainly affects the end of the track. In the details of Front-N, there is a difference in the area extension, as evidenced by the fact that more Front-N are located south of Australia and New Zealand at the results of track data sets with a finer spatial resolution (Fig. 9c-d). Different spatial resolution schemes have more divergence in the identification of cyclone track points in these regions, especially the track points at the beginning. In the details of Back-N, there is an extra high values region at the westward of Andes, indicating that the shared tracks experience different degrees of terrain influence at different spatial resolutions. In comparison, the temporal resolution has little effect on the track of shared cyclones. Fewer additional points were gained by increasing temporal resolution, on average less than 5%. It is worth noting that the results of Figure 9 also depend on the pairing rate in Figure 7. A track data set with a high pairing rate

is likely to have more proportion of additional track points, which explains the fact that the proportion of additional track points is larger in the results of 6hT63 and 3hT42 track data sets.

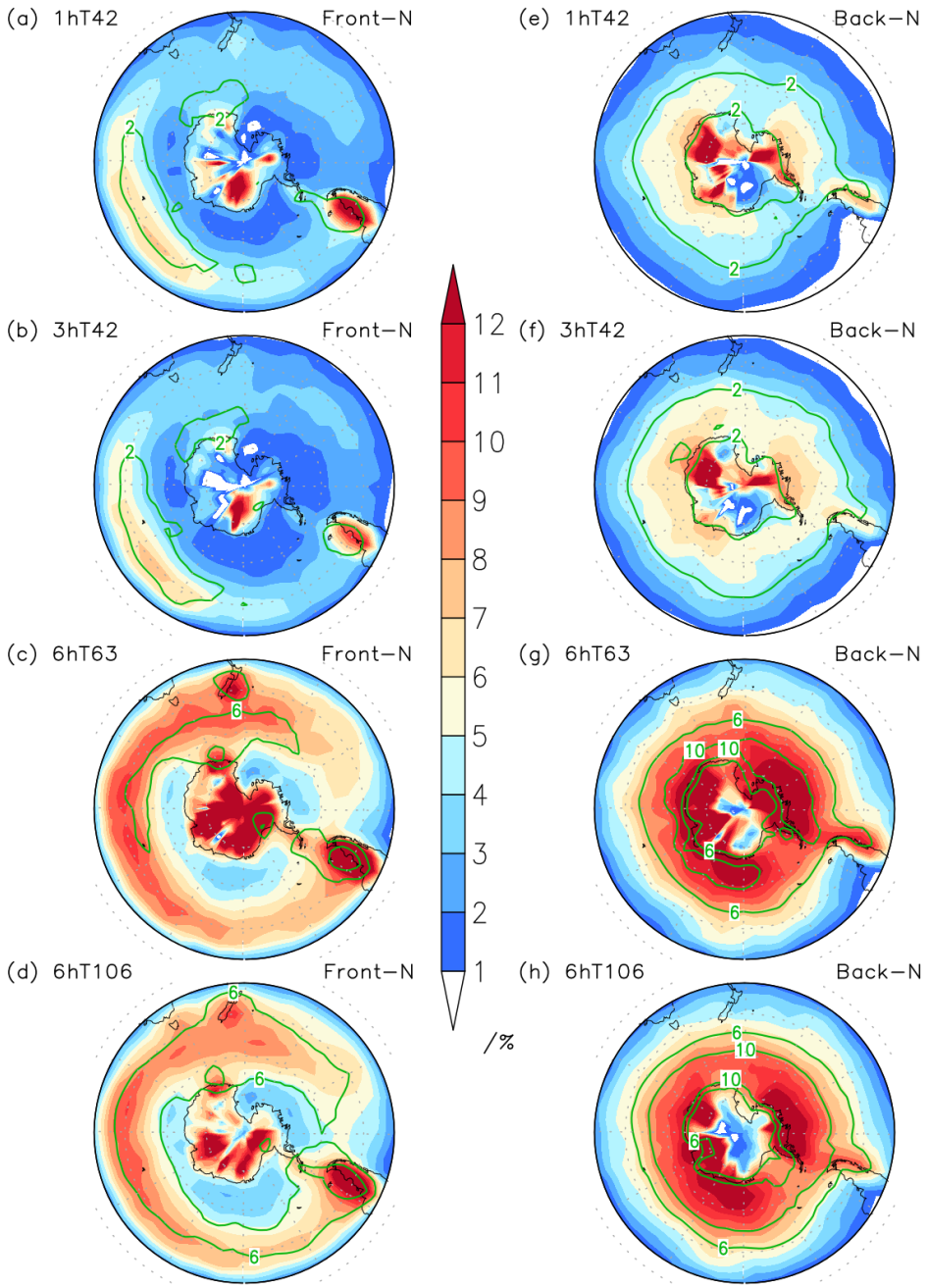

Fig. 9. The spatial feature pattern of additional track points (track points during the overlap period have been removed) of shared cyclones in track data sets with high resolution and 6hT42 track data set. The track points before the overlap time are shown in (a-d) and the track points after the overlap time are shown in (e-h). The shaded shows the percentage of additional track points based on Figure 5 and the contour is the number of additional track points counted in a 500 km radius around grid points per year. The number of additional track points is normalized.

The shared cyclones of different track data sets generally have different characteristics. Figure 10 compares the characteristics of shared cyclones in the reference 6hT42 track data set with that in the track data sets that have finer temporal or spatial resolutions. Most of the points fall on the red line, indicating the minimum MSLP of most shared cyclones is equal in the two-track data sets. But there are still some MSLP points away from the red line and the lower half of the triangle is more than the upper half, indicating that the strength of some shared cyclones in the 6hT42 track data set is greater than that in other track data sets. Some of the MSLP points deviate significantly from the red line. One reason is that only the minimum pressure values of the tracks are taken here for comparison for the shared cyclones that may have multiple intensification processes and multiple pairs. Except for this, the tracked centers may be in different locations from which the MSLP search proceeds so different minima may be found. In contrast, for cyclone lifetimes, there are more points in the upper half of the triangle than in the lower half, except for the results between 3hT42 and 6hT42. The impact of spatial and temporal resolution on the lifetime and moving distance of cyclones are significant. There are more dispersed points for the lifetime and moving distance of shared cyclones in the track data sets with different spatial resolutions. The mean speed of shared cyclones of different track data sets shows good upper and lower symmetry around the red line, which means that it has less sensitivity to spatiotemporal resolution. The probability of increasing or decreasing cyclone speed caused by spatiotemporal resolution is similar. In addition, the similarity of shared cyclones between the track data sets with the same spatial resolution is larger than that with the same temporal resolution, which is reflected in more feature points falling on the red line and less dispersed points. In general, the spatial resolution has a greater impact on the characteristics of shared cyclones than temporal resolution.

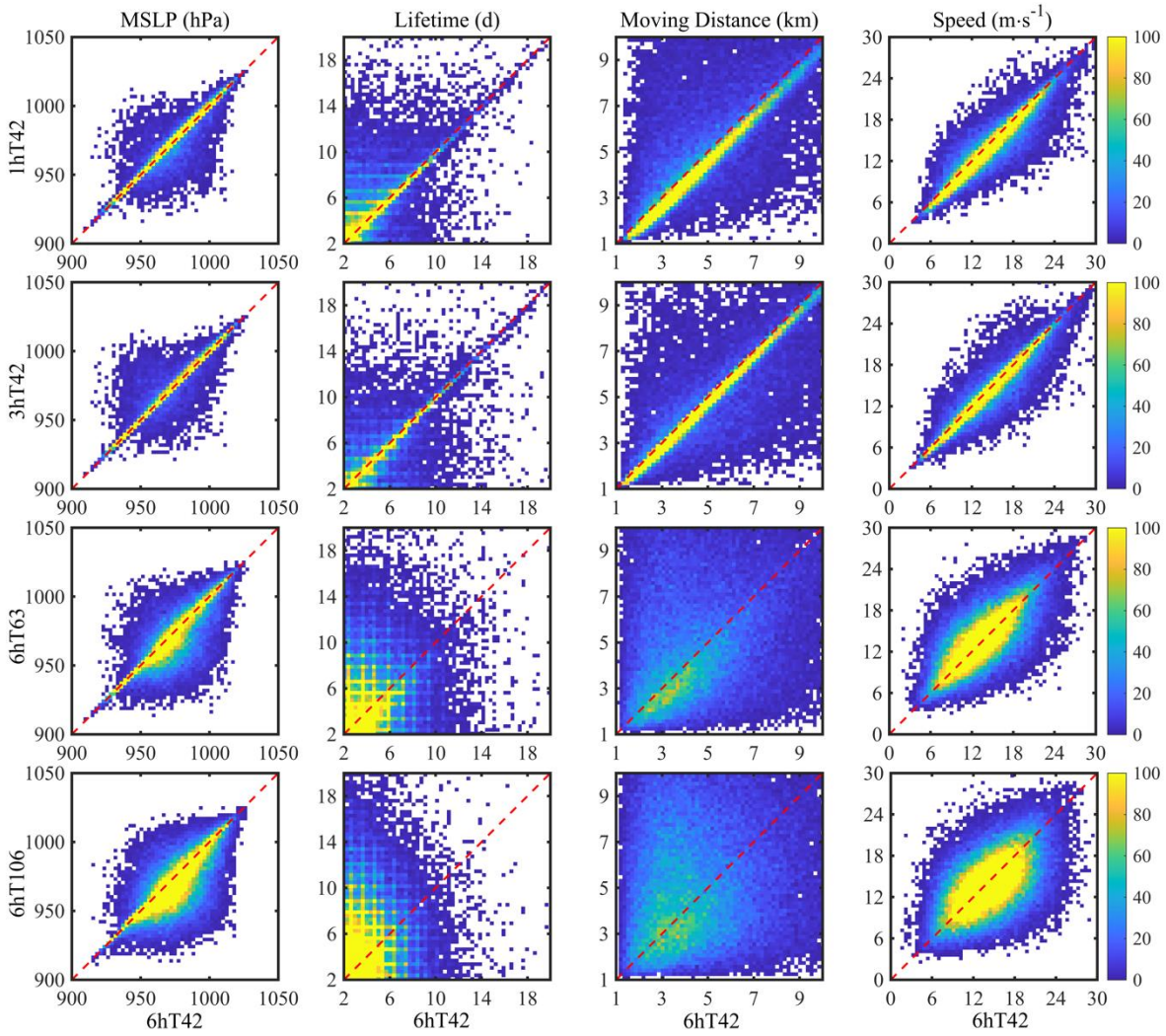

Fig. 10. The scatter of the cyclone features of the shared cyclones in different track data sets. The minimum MSLP is shown in the first column. The lifetime is shown in the second column. The moving distance is shown in the third column and the translation speed is in the fourth column. The first row is the results between 1hT42 and 6hT42 track data sets. Similarly, the 2~4 rows are the results between other track data sets and the 6hT42 track data set. Scatter density is given colors. The red dash line is the reference line with equal horizontal and vertical values.

Table. 2 shows the mean values of the shared cyclone features from different track data sets. The shared cyclone has a similar feature in the track data sets with the same spatial resolution but the moving distance of that from 3hT42 is 300 km longer than the results of 6hT42. The increase in spatial resolution will largely decrease the lifetime and the moving distance of cyclones. The mean lifetime of shared cyclones in 6hT106 track data sets is 36h shorter than the results of 6hT42, corresponding to the reduction of an average moving distance of 1500 km. For the shared cyclones, the minimum MSLP and speed are less sensitive to the data resolution.

Table 2. Comparison of mean values of shared cyclone features. The number is the mean values of shared cyclone features from the track data sets with higher resolution and the number in the brackets are the corresponding values from the 6hT42 track data sets.

	MSLP (hPa)	Lifetime (h)	Moving distance (km)	Speed ($m \cdot s^{-1}$)
1hT42-6hT42	969 (969)	107 (116)	5405 (5569)	14.4 (13.8)
3hT42-6hT42	970 (970)	112 (110)	5570 (5287)	14.2 (13.8)
6hT63-6hT42	970 (968)	104 (122)	5003 (5961)	13.7 (13.9)
6hT106-6hT42	971 (967)	94 (130)	4798 (6334)	14.5 (14.0)

4. Conclusion and Discussion

a. Conclusion

Based on the high-resolution ERA5 reanalysis data, this paper obtains track data sets of cyclones over the Southern Ocean by pre-processing the 850 vorticities at different spatial and temporal resolutions. The results show that there are more tracks in the track data sets with high spatial resolution but fewer tracks in the track data sets with high temporal resolution. On one hand, high spatial resolution preserves more noise which will lead to more broken tracks. On the other hand, the results of high spatial resolution also contain more mesoscale or small-scale cyclones increasing the total number of tracks. In contrast, the identification of transition points between two adjacent tracks is different in different temporal resolutions, which decide the split and merge of tracks. More importantly, the shorter lifetime and moving distance of the cyclones from the track data sets obtained by high temporal resolution make them more difficult to pass the filtering conditions of the algorithm leading to a reduction in the total number.

Further investigation of the features of cyclones in detail shows the frequency distribution of features is consistent among schemes and shows similar seasonal variation at the same spatial resolution, although there are large differences in the mean value of minimum MSLP, lifetime, and moving distance for track data sets obtained by different spatial resolutions. It is revealed that the statistical results of cyclone features are strongly affected by the resolution of the input data. Seasonal variation is also found in the peak latitude of cyclogenesis that shifts north in the cold season and south in the warm season. The cyclogenesis locations and active areas have strong consistency among the results of different schemes. There are four main cyclogenesis regions: the eastern coastal region of South America (50-70°W, 40-55°S), northwest off Adélie Land coast (140~160°E, 60~70°S), over New Zealand (170-180°E, 40-

50°S), and center of Southern Indian Ocean (60-110°E, 45-55°S). The cyclones formed in these areas create an annular active area along the coast of Antarctica, with two high-frequency areas: the region (90°E-120°W, 60-65°S) and west of the Antarctic Peninsula. Most cyclones over the Southern Ocean move southeast around the pole after cyclogenesis leading to a high-density area of track points along the coast of Antarctica. The translation speed of cyclones plays an important role in the latitudinal inhomogeneity of the spatial density of track points. The cyclone speed is influenced by the topography and background wind in these areas.

The influence of resolution on individual cyclones is not clear from the statistical results above because of the contribution of a large number of additional cyclones to the mean values, which can be solved by track matching methods. During the pairing process, we found that there are multiple pairs when matching two track data sets obtained by different spatiotemporal resolution pre-processing schemes. The proportion of multiple pairs is about 5 % (the same spatial resolution) and 5~40 % (different spatial resolution), which also depended on the choice of baseline track data set. Previous track matching methods have limitations when pairing the tracks with large differences in lifetimes or could not find the best match pair for each track that may affect the comparison of cyclones' characteristics. It was necessary to provide a new track matching method that combines the advantage of previous methods for this study. It has a "closest to each other" criteria to obtain the best match pairs and get as many as possible multiple pairs through a recursive procedure which can help to reduce false negatives. The suitable distance thresholds of the new track method and a fixed period of overlap allow for wider applicability to a greater variety of cyclone track data sets.

After separating the shared tracks and additional tracks by the track matching method, a study of the features of shared tracks further reveals the effects of higher resolution. For the shared tracks, additional track points of the tracks from high resolution can be divided into two groups before and after the overlapping time that has a different distribution pattern. The number of additional track points after the overlapping time is larger than that before the overlapping time. There are great differences in the identification of cyclone track points in some regions with different spatial resolutions, compared with different temporal resolutions. In addition, the sensitivity of cyclone characteristics to temporal and spatial resolution is different. The comparison between the scatter of points about the diagonal red line and those in the upper and lower triangle shows the characteristic differences of the shared cyclone in

683 different track data sets. This detailed comparison of shared tracks demonstrates the influence
684 of high-resolution schemes, providing a reference to the user and designer of the objective
685 tracking algorithms in the decision of the data resolution used in the tracking.

686 *b. Discussion*

687 Although we have compared six track data sets of cyclones obtained by pre-processing
688 schemes with different spatiotemporal resolutions in detail, it is difficult to evaluate which
689 scheme is the best. For example, the track lengths and lifetime of the cyclones in the 3hT42
690 scheme are longer than those in other schemes. Some tracks still have anomalous large
691 steering for some cases in the 3hT42 scheme. However, the results of the 3hT42 scheme have
692 a high pairing rate with the commonly used 6hT42 scheme, and we have no evidence that the
693 tracks obtained by the 3hT42 scheme are wrong. An important reason for this puzzle is that a
694 universally recognized “Best track” for extratropical cyclones does not exist. Even if it
695 existed, it would have errors and biases just like the TC Best Track (Schreck et al. 2014). The
696 number of extratropical cyclones is much more than that of tropical cyclones, making a case-
697 by-case analysis more difficult. The results of various algorithms are still very different, and
698 some cyclone characteristics vary greatly between different schemes (Neu et al. 2013).
699 Although we can manually evaluate the results of automatic tracking, the manual evaluation
700 is subjective, two observers might still produce different results. For these reasons, it is hard
701 to distinguish which track data sets obtained in this study best fit the actual situation. Despite
702 some differences between the results of various schemes, it is reassuring to know that most
703 cyclone features, including the spatial distribution of cyclogenesis and activity regions, the
704 annual trend, and seasonal variation of intensity and lifetime, are similar among schemes
705 apart from differences in track numbers due to different spatial resolutions. This gives us
706 some confidence to use high-resolution schemes in other studies. Finding suitable settings for
707 different resolution schemes is also quite a rewarding work that can be tested in both
708 hemispheres.

709 Increased spatial resolution in the pre-processing allows for more accurate localization of
710 cyclone centers and brings greater vorticity (after spectral filtering) of the same cyclone as
711 well. The intensity of the track points is more likely to meet algorithmic thresholds and
712 therefore capture weak cyclones better. However, there is more noise retention, which makes
713 the tracks easier to split or merge. Additional and subjective criteria are required to address
714 this problem (Hanley and Caballero 2012; Souders et al. 2014). The finer spatial resolution

brings a significant increase in the number of cyclones. These additional cyclones are distributed throughout the Southern Ocean, especially along the coast of Antarctica and near the 35 °S boundaries. They might be small-scale cyclones (mesocyclones) or associated with large vorticity regions such as shear zones which could be discriminated by adding other fields to the tracks. The reasons for the cyclogenesis of additional cyclones over different regions and different seasons can be different, which needs further investigation.

The finer temporal resolution can better identify the start and end positions of the track while increasing the uncertainty of the track. The track shown in Figure 6 is a good example. One track at 1hT42 and 3hT42 track data set match with two tracks at 6hT42 track data set. It is hard to determine whether it is one cyclone or two cyclones. There are many types of cyclones and some types can be transformed into others. Interactions between multiple neighboring systems and the influence of topography can also cause cyclones to weaken and intensify in stages, making one cyclone look like two. Thus, when we have finer resolution reanalysis data or model data, it is not recommended to directly use a high-resolution preprocessing scheme. We should select a suitable scheme according to the study area and the size of the target cyclones. The track data set allows for some following quality control, through further study of the cyclone intensifications, splitting and merging phenomena of cyclones.

The differences between the tracking at different resolutions also depend on the subjective choice of the tracking parameters, which are resolution-dependent, as well as the resolutions themselves. The choice has to be a trade-off between too loose constraints and too strict constraints, both of which can lead to tracking errors. One example of this is the wide range of maximum displacement distances in a time step used in previous studies (Gramcianinov et al. 2020).

The choice of field that is used in the tracking can also introduce uncertainty between track data sets and it will also affect the resolutions that can be used. T42 is a low resolution if using MSLP but is a suitable resolution if using vorticity. Before comparing the results of different tracking algorithms, the appropriate resolution needs to be chosen for the fields they use. Using T106 with MSLP is more comparable with using vorticity at T42 and T63 (Jung et al. 2012). In addition, we use ξ_{850} for tracking and show the sensitivity to data resolution in this study. It is also worth tracking at other levels and figuring out the influence of data resolution on the tracking of upper-level cyclones, such as mid-troposphere and upper-troposphere cyclones.

In this study, a new track matching method has been developed and tested. It removes as many unnecessary constraints as possible and captures all possible pairs, especially for multiple pairs. It solves the problem of pairing two cyclones with large differences in their lifetime. This method can be used to compare the track sets obtained by different input data, input variables, and different algorithms. It can also be used in the test and improvement of the same tracking algorithm, which is of great benefit to the study of cyclone regional characteristics and the improvement of the cyclone tracking algorithm. But special attention needs to be paid to the influence of boundaries on the track-matching of regional cyclones. Some cyclones move across boundaries, which can lead to an underestimation of cyclone pairing rates near boundaries. The spatial and temporal resolution affects the lifetime and moving distance of the cyclones. Some pairable cyclones in some track data sets will be removed by the user's chosen filtering condition but they still exist in other track data sets. They cannot be correctly calculated in the pairing rate, resulting in a bias in the pairing rate.

Acknowledgments.

This study is supported by the National Natural Science Foundation of China (No. 41941009, 41922044), and the Fundamental Research Funds for the Central Universities (No. 19lgzd07). The authors would like to thank European Centre for Medium-Range Weather Forecasts for providing ERA-5 reanalysis data and are grateful to the editor and Alex Crawford, University of Manitoba, and another anonymous reviewer for their helpful comments and suggestions.

Data Availability Statement.

Input data from ERA5 are available at https://cds.climate.copernicus.eu/cdsapp#!/home. Code for the cyclone detection and tracking algorithm (Track-1.5.2) can be found at https://gitlab.act.reading.ac.uk/track/track.

REFERENCES

Allen, J. T., A. B. Pezza, and M. T. Black, 2010: Explosive cyclogenesis: A global climatology comparing multiple reanalyses. *J. Climate*, **23**, 6468-6484.

Alpert, P., B. U. Neeman, and Y. Shayel, 1990: Climatological analysis of the Mediterranean cyclones using ECMWF data. *Tellus A*, **42**, 65-77.

781 Bauer, M., G. Tselioudis, and W. B. Rossow, 2016: A New Climatology for Investigating
782 Storm Influences in and on the Extratropics. *J. of Applied Meteor. and Climatology*, **55**,
783 1287-1303.

784 Berrisford, P., P. Kållberg, S. Kobayashi, D. Dee, S. Uppala, A. J. Simmons, P. Poli, and H.
785 Sato, 2011: Atmospheric conservation properties in ERA-Interim. *Quart. J. Roy. Meteor.*
786 *Soc.*, **137**, 1381–1399.

787 Blender, R., K. Fraedrich, and F. Lunkeit, 1997: Identification of cyclone-track regimes in the
788 North Atlantic. *Quart. J. Roy. Meteor. Soc.*, **123**, 727-741.

789 Blender, R., and M. Schubert, 2000: Cyclone Tracking in Different Spatial and Temporal
790 Resolutions. *Mon. Wea. Rev.*, **128**, 377-384.

791 Boer, G.J., 1995. Some dynamical consequences of greenhouse gas warming. *Atmos.-Ocean*,
792 **33**, 731e751.

793 Bromwich, D. H., R. L. Fogt, K. I. Hodges, and J. E. Walsh, 2007: A tropospheric assessment
794 of the ERA-40, NCEP, and JRA-25 global reanalyses in the polar regions. *J. Geophys.*
795 *Res.*, **112**, D10111.

796 Bromwich, D. H., D. F. Steinhoff, I. Simmonds, K. Keay, and R. L. Fogt, 2011:
797 Climatological aspects of cyclogenesis near Adélie Land Antarctica. *Tellus A: Dynamic*
798 *Meteorology and Oceanography*, **63**, 921-938.

799 Carleton, A. M., 1979: A synoptic climatology of satellite observed extratropical cyclone
800 activity for the Southern Hemisphere winter. *Arch. Met. Geophys. Biokl. B.*, **27**, 265-279.

801 Carrasco, J. F., D. H. Bromwich, and A. J. Monaghan, 2003: Distribution and characteristics
802 of mesoscale cyclones in the Antarctic: Ross Sea eastward to the Weddell Sea. *Mon. Wea.*
803 *Rev.*, **131**, 289–301.

804 Chen, S. L. Zhang, and C. Lu, 1989: A statistical analysis of cyclone tracks in west antarctic
805 region (In Chinese). *J. Acad. of Meteor. Sci.*, **2**, 150-155.

806 Claud, C., A. M. Carleton, B. Duchiron, and P. Terray, 2009: Southern hemisphere winter
807 cold-air mesocyclones: climatic environments and associations with teleconnections.
808 *Climate Dyn.*, **33**, 383–408.

809 Crawford, A. D., E. A. P. Schreiber, N. Sommer, M. C. Serreze, J. C. Stroeve, and D. G.
810 Barber, 2021: Sensitivity of Northern Hemisphere Cyclone Detection and Tracking

Results to Fine Spatial and Temporal Resolution Using ERA5. *Mon. Wea. Rev.*, **149**, 2581-2598.

Di Luca, A., J. P. Evans, A. Pepler, L. Alexander, and D. Argüeso, 2015: Resolution sensitivity of cyclone climatology over eastern Australia using six reanalysis products. *J. Climate*, **28**, 9530-9549.

Dowdy, A.J., A. Pepler, A. Di Luca, L. Cavicchia, G. Mills, J. P. Evans, S. Louis, K. L. Mclnnes, and K. Walsh, 2019: Review of Australian east coast low pressure systems and associated extremes. *Climate Dyn.*, **53**, 4887–4910.

Flaounas, E., V. Kotroni, K. Lagouvardos, and I. Flaounas, 2014: CycloTRACK (v1.0)-tracking winter extratropical cyclones based on relative vorticity: Sensitivity to data filtering and other relevant parameters. *Geosci. Model Dev.*, **7**, 1841-1853.

Gramcianinov C. B., K. I. Hodges, and R. Camargo, 2019: The properties and genesis environments of South Atlantic cyclones. *Climate Dyn.*, **53**, 4115-4140.

Gramcianinov C. B., R. M. Campos, R. de Camargo, K. I. Hodges, C. Guedes Soares, and P. L. da Silva Dias, 2020: Analysis of Atlantic extratropical storm tracks characteristics in 41 years of ERA5 and CFSR/CFSv2 databases. *Ocean Eng.*, **216**, 108111.

Grieger, J, G. C. Leckebusch, C. C. Raible, I. Rudeva, and I. Simmonds, 2018: Subantarctic cyclones identified by 14 tracking methods, and their role for moisture transports into the continent. *Tellus A: Dynamic Meteorology and Oceanography*, **70**, 1-18.

Haak, U., and U. Ulbrich, 1996: Verification of an objective cyclone climatology for the North Atlantic. *Meteor. Z.*, **5**, 24-30.

Hanley, J. and R. Caballero, 2012: Objective identification and tracking of multicentre cyclones in the ERA-Interim reanalysis dataset. *Quart. J. Roy. Meteor. Soc.*, **138**, 612-625.

Hersbach, H., B. Bell, P. Berrisford, et al., 2020: The ERA5 global reanalysis. *Quart. J. Roy. Meteor. Soc.*, **146**, 1999-2049.

Hewson, T. D., 1998: Objective fronts. *Meteor. Appl.*, **5**, 37-65.

Hodges, K. I., 1994: A general method for tracking analysis and its application to meteorological data. *Mon. Wea. Rev.*, **122**, 2573-2586.

Hodges, K. I., 1995: Feature tracking on the unit sphere. *Mon. Wea. Rev.*, **123**, 3458-3465.

841 Hodges, K. I., 1999: Extension of spherical nonparametric estimators to nonisotropic kernels:
842 An oceanographic application. *Mon. Wea. Rev.*, **127**, 214-227.

843 Hodges, K. I., B. J. Hoskins, J. Boyle, and C. Thorncroft, 2003: A Comparison of Recent
844 Reanalysis Datasets Using Objective Feature Tracking: Storm Tracks and Tropical
845 Easterly Waves. *Mon. Wea. Rev.*, **131**, 2012-2037.

846 Hodges, K. I., R. W. Lee, and L. Bengtsson, 2011: A comparison of extratropical cyclones in
847 recent reanalyses ERA-Interim, NASA MERRA, NCEP CFSR, and JRA-25. *J. Climate*,
848 **24**, 4888-4906.

849 Hoskins, B. J., and K. I. Hodges, 2002: New perspectives on the Northern Hemisphere winter
850 storm tracks. *J. Atmos. Sci.*, **59**, 1041-1061.

851 Hoskins, B.J., Hodges, K.I., 2005. A new perspective on southern hemisphere storm tracks. *J.*
852 *Climate*, **18**, 4108-4129.

853 Jones D. A., and I. Simmonds, 1993: A climatology of Southern Hemisphere extratropical
854 cyclones. *Climate Dyn.*, **9**, 131-145.

855 Jung, T., S. K. Gulev, and I. Rudeva, 2006: Sensitivity of extratropical cyclone characteristics
856 to horizontal resolution in the ECMWF model. *Quart. J. Roy. Meteor. Soc.*, **132**, 1839-
857 1857.

858 Jung, T., M. J. Miller, T. N. Palmer, P. Towers, N. Wedi, D. Achuthavarier, J. M. Adams, E.
859 L. Altshuler, B. A. Cash, J. L. Kinter III, L. Marx, C. Stan, and K. I. Hodges, 2012: High-
860 Resolution Global Climate Simulations with the ECMWF Model in Project Athena:
861 Experimental Design, Model Climate, and Seasonal Forecast Skill, *J. Climate*, **25**, 3155-
862 3172.

863 König, W., R. Sausen, and F. Sielmann, 1993: Objective identification of cyclones in GCM
864 simulations. *J. Climate*, **6**, 2217-2231.

865 Lakkis, G., P. Canziani, A. Yuchechen, L. Rocamora, A. Caferri, K. I. Hodges, and A.
866 O'Neill, 2019: A 4D feature tracking algorithm: a multidimensional view of cyclone
867 systems. *Quart. J. Roy. Meteor. Soc.*, **145**, 395-417.

868 Meehl, G. A. (1991), A reexamination of the mechanism of the semiannual oscillation in the
869 Southern Hemisphere. *J. Climate*, **4**, 911– 926.

Murray R. J., and I. Simmonds, 1991: A numerical scheme for tracking cyclone centers from digital data. Part I: Development and operation of the scheme. *Aust. Meteor. Mag.*, **39**, 155-166.

Nakamura, H., and A. Shimpo, 2004: Seasonal variations in the Southern Hemisphere storm tracks and jet streams as revealed in a reanalysis dataset. *J. Climate*, **17**, 1828–1844.

Neu, U., and Coauthors, 2013: IMILAST: A Community Effort to Intercompare Extratropical Cyclone Detection and Tracking Algorithms. *Bull. Amer. Meteor. Soc.*, **94**, 529-547.

Physick, W. L., 1981, Winter depression tracks and climatological jet streams in the southern hemisphere during the FGGE year. *Quart. J. Roy. Meteor. Soc.*, **107**, 883-898.

Pinto, J. G., T. Spangehl, U. Ulbrich, and P. Speth, 2005: Sensitivities of a cyclone detection and tracking algorithm: Individual tracks and climatology. *Meteor. Z.*, **14**, 823-838.

Raible, C. C., P. M. Della-Marta, C. Schwierz, H. Wernli, and R. Blender, 2008: Northern Hemisphere extratropical cyclones: A comparison of detection and tracking methods and different reanalyses. *Mon. Wea. Rev.*, **136**, 880-897.

Rohrer, M., O. Martius, C. C. Raible, and S. Brönnimann, 2020: Sensitivity of Blocks and Cyclones in ERA5 to Spatial Resolution and Definition. *Geophys. Res. Lett.*, **47**, e2019GL085582.

Rudeva, I., S. K. Gulev, I. Simmonds, and N. Tilinina, 2014: The sensitivity of characteristics of cyclone activity to identification procedures in tracking algorithms. *Tellus*, **66A**, 24961.

Schreck, C. J., III, K. R. Knapp, and J. P. Kossin, 2014: The Impact of Best Track Discrepancies on Global Tropical Cyclone Climatologies using IBTrACS. *Mon. Wea. Rev.*, **142**, 3881-3899.

Schubert, M., J. Perlwitz, R. Blender, K. Fraedrich, and F. Lunkeit, 1998: North Atlantic cyclones in CO2-induced warm climate simulations: Frequency, intensity, and tracks. *Climate Dyn.*, **14**, 827-838.

Schultz, D. M., L. F. Bosart, B. A. Colle, H. C. Davies, C. Dearden, D. Keyser, O. Martius, P. J. Roebber, W. J. Steenburgh, H. Volkert, and A. C. Winters, 2019: Extratropical Cyclones: A Century of Research on Meteorology's Centerpiece. *Meteor. Monogr.*, **59**, 16.1-16.56.

Serreze, M. C., 1995: Climatological aspects of cyclone development and decay in the Arctic. *Atmos. -Ocean*, **33**, 1-23.

Simmonds, I., Keay, K. and Lim, E.-P. 2003. Synoptic activity in the seas around Antarctica. *Mon. Wea. Rev.*, **131**, 272–288.

Simmonds, I. C. Burke, and K. Keay, 2008: Arctic climate change as manifest in cyclone behavior. *J. Climate*, **21**, 5777-5796.

Sinclair, M. R., 1994: An objective cyclone climatology for the Southern Hemisphere. *Mon. Wea. Rev.*, **122**, 2239-2256.

Sinclair, 1995: A climatology of cyclogenesis for the Southern Hemi- sphere. *Mon. Wea. Rev.*, **123**, 1601–1619.

Sinclair, M. R., 1997: Objective identification of cyclones and their circulation intensity, and climatology. *Wea. Forecasting*, **12**, 595-612.

Souders, M. B., B. A. Colle, and E. K. M. Chang, 2014: A Description and Evaluation of an Automated Approach for Feature-Based Tracking of Rossby Wave Packets, *Mon. Wea. Rev.*, **142**, 3505-352.

Streten, N. A., and A. J. Troup, 1973: A synoptic climatology of satellite observed cloud vortices over the Southern Hemisphere. *Quart. J. Roy. Meteor. Soc.*, **99**, 56-72.

Taljaard, J. J., 1965: Cyclogenesis, clones and anticyclones in the Southern Hemisphere during the period June to December 1958. *Notos*, **14**, 73-84.

Taljaard, J. J., 1967: Development, distribution and movement of cyclones and anticyclones in the Southern Hemisphere during the IGY. *J. Appl. Met.*, **6**, 973-987.

Tilinina, N., S. K. Gulev, I. Rudeva, and P. Koltermann, 2013: Comparing cyclone life cycle characteristics and their interannual variability in different reanalyses. *J. Climate*, **26**, 6419-6438.

Turner, J., G. J. Marshall, and T. A. Lachlan-Cope, 1998: Analysis of synoptic-scale low pressure systems within the Antarctic Peninsula sector of the circumpolar trough. *Int. J. Climatol.*, **18**, 253-280.

Ueno, K., 1993: Interannual variability of surface cyclone tracks, atmospheric circulation patterns, and precipitation patterns in winter. *J. Meteor. Soc. Japan*, **71**, 655-671.

Vessey, A. F., K. I. Hodges, L. C. Shaffrey, and J. J. Day, 2020: An inter-comparison of Arctic synoptic scale storms between four global reanalysis datasets. *Climate Dyn.*, **54**, 2777-2795.

Wang, X. L., Y. Feng, R. Chan, and V. Isaac, 2016: Inter-comparison of extra-tropical cyclone activity in nine reanalysis datasets. *Atmos. Res.*, **181**, 133-153.

Wei, L., and T. Qin. 2016. Characteristics of cyclone climatology and variability in the Southern Ocean. *Acta Oceanol. Sin.*, **35**, 59-67.

Wernli, H., and C. Schwierz, 2006: Surface cyclones in the ERA-40 dataset (1958-2001). Part I: Novel identification method and global climatology. *J. Atmos. Sci.*, **63**, 2486-2507.

Xia, L., M. Zahn, K. I. Hodges, F. Feser, and H. Storch, 2012: A comparison of two identification and tracking methods for polar lows. *Tellus A*, **64**, 17196.

Yuan, X., J. Patoux, and C. Li, 2009: Satellite-based midlatitude cyclone statistics over the Southern Ocean: 2. Tracks and surface fluxes. *J. Geophys. Res.*, **114**, D04106.

Zappa, G., L. Shaffrey, and K. I. Hodges, 2014: Can Polar Lows be Objectively Identified and Tracked in the ECMWF Operational Analysis and the ERA-Interim Reanalysis?. *Mon. Wea. Rev.*, **142**, 2596-2608.